JAAS

Accepted Manuscript

This is an *Accepted Manuscript*, which has been through the Royal Society of Chemistry peer review process and has been accepted for publication.

Accepted Manuscripts are published online shortly after acceptance, before technical editing, formatting and proof reading. Using this free service, authors can make their results available to the community, in citable form, before we publish the edited article. We will replace this *Accepted Manuscript* with the edited and formatted *Advance Article* as soon as it is available.

You can find more information about *Accepted Manuscripts* in the Information for Authors.

Please note that technical editing may introduce minor changes to the text and/or graphics, which may alter content. The journal's standard Terms & Conditions and the Ethical guidelines still apply. In no event shall the Royal Society of Chemistry be held responsible for any errors or omissions in this *Accepted Manuscript* or any consequences arising from the use of any information it contains.

ROYAL SOCIETY OF CHEMISTRY

www.rsc.org/jaas

Journal Name

RSCPublishing

ARTICLE

Analysis of relative standard deviation of spectral line intensity and intensity ratio in laser-induced breakdown spectroscopy using $CuIn_{1-x}Ga_xSe_2$ thin film sample

Cite this: DOI: 10.1039/x0xx00000x

Received 00th January 2012,
Accepted 00th January 2012

DOI: 10.1039/x0xx00000x

www.rsc.org/

Jung-Hwan In, Chan-Kyu Kim and Sungho Jeong

The precision of laser induced breakdown spectroscopy (LIBS) measurement is influenced by both the shot noise of detector and the shot-to-shot fluctuation noise of laser plasma. Since both types of noise are related to the variation of photon number, it is hard to clearly estimate the degree of influence by each noise on the measured LIBS signal. In this work, to quantitatively estimate the shot noise of an intensified charge-coupled device detector, a model in which the detector noise is linearly correlated to signal intensity is developed. Using a stable light source for intensity calibration, the correlation parameter of detector noise is determined. By subtracting the relative standard deviation (RSD) of detector shot noise from the RSD of measured LIBS signal intensity or intensity ratio, the variation of RSD due to plasma fluctuation alone was obtained. From LIBS analysis of $CuIn_{1-x}Ga_xSe_2$ thin film at various experimental conditions (laser energy: 0.16 ~ 2.9 mJ, gate delay: 0.12 ~ 3.6 μs, spot size: 42 and 104 μm), it was found that the plasma-fluctuation-induced RSD of absolute intensity tended to increase with gate delay and to decrease with laser fluence. The plasma-fluctuation-induced RSD of intensity ratio, however, tended to initially decrease with gate delay to a minimum value before starting to increase at longer gate delay. The observed behavior of plasma-fluctuation-induced RSD of intensity ratio is understood to be related to the spectral properties of emission lines and elements of interest.

Introduction

The application of laser induced breakdown spectroscopy (LIBS) to industry for process monitoring during thin film manufacturing, metal scrap sorting, liquid slag analysis, drill dust analysis, coal ash content monitoring, etc.[1-8] has been expanding recently due to its intrinsic advantages of no sample preparation, in-air measurement and rapid analysis[9,10]. In LIBS analysis, measurement parameters (laser energy, gate delay, gate width, etc.) are optimized typically into a direction to improve the limit of detection and/or to minimize relative standard deviation (RSD)[2,11-20]. For an application in which the analysis of major elements is concerned such as the concentrations of Cu, In, Ga, and Se in $CuIn_{1-x}Ga_xSe_2$ (CIGS) thin film solar cell, the improvement of precision by minimizing RSD is more important than limit of detection[2]. The RSD of LIBS signal may be roughly classified into detector noise (shot noise + dark current noise + readout noise)[21] and shot-to-shot plasma fluctuation noise (flicker noise). Detector noise is governed by input photon number (shot noise), detector sensor temperature (dark current noise), and the configuration for signal amplification. For an intensified charge coupled device (ICCD) detector, dark current noise and readout noise are negligible and thus shot noise dominates the detector noise[21]. Generally, shot noise is known to decrease with the increase of input photon number[22]. On the other hand, plasma fluctuation noise due to the stochastic shot-to-shot variation of laser-material interaction and/or the fluctuation of plasma evolution is closely related to measurement conditions like laser energy, gate delay, gate width, etc. Because a change in measurement conditions also causes shot noise change, precision analysis of LIBS signal in previous studies was typically done for the resultant RSD rather than the individual contribution of detector noise or plasma fluctuation noise[6,10-14]. Although limited, however, study for the behavior of individual noise source influencing the precision of LIBS data is increasing recently. For example, from the analysis of 750-shot LIBS data of steel sample, Mermet et al.[22] identified that drift was the main contribution to RSD. To improve the precision of LIBS measurement, it is necessary to systematically examine the variation of plasma fluctuation noise with respect to major LIBS measurement parameters.

In this study, the variation of RSD due to plasma fluctuation with respect to signal intensity and major measurement parameters (laser pulse energy, spot diameter, and detector gate delay) is investigated. The RSD of plasma fluctuation noise was isolated from the RSD of overall signal by subtracting the shot noise component estimated with an experimental model for

ICCD detector. Using the LIBS data of CIGS thin film, the variation of RSDs of absolute intensities or intensity ratios due to plasma fluctuation was examined with respect to signal intensity and measurement conditions.

Theory

Shot noise of ICCD

Fig. 1(a) shows a schematic diagram of the LIBS setup that adopts an ICCD detector. The photons emitted from the laser plasma are collected by the collection lens and delivered via an optical fiber bundle to the spectrometer. The dispersed light is then amplified in the ICCD consisting of a photocathode, multichannel plate (MCP), and phosphor screen as shown in Fig. 1(b). Provided that the photons falling onto the photocathode is assumed to have a delta-function like spatial profile, the spatial distribution of photons incident on the CCD would become broadened during the amplifying process as illustrated in Fig. 1(b)[23]. The amplified photons are then stored in the CCD as charges, the observed signal. Then, the stored charge number (S) (or the signal intensity) in the whole CCD columns can be represented by

$$S = JQ_{pc}GEQ_{CCD} \tag{1}$$

where J is the number of photons within the delta-function like spatial profile, Q_{pc} is quantum efficiency of the photocathode, G is gain of the MCP, E is an electron-photon conversion efficiency of the phosphor screen, and Q_{CCD} is quantum efficiency of the CCD detector.

In a cascade system like ICCD, noise of the stored charge number is determined by the probability distribution at each stage (J, Q_{pc}, G, E, and Q_{CCD}). Provided that dark current noise and readout noise are negligible but photon noise (shot noise) is dominant, the variance (σ_S^2) of stored charge number can be expressed by Burgess' variance theorem[24, 25] as

$$\begin{aligned}\sigma_S^{\,2} &= \left(\sigma_J Q_{pc} GEQ_{CCD}\right)^2 + J\left(\sigma_{Q_{pc}} GEQ_{CCD}\right)^2 \\ &+ JQ_{pc}\left(\sigma_G EQ_{CCD}\right)^2 + JQ_{pc}G\left(\sigma_{EQ_{CCD}}\right)^2\end{aligned} \tag{2}$$

Since it can be assumed that the number distribution of J has the Poisson distribution ($\sigma_J^{\,2} = J$), Q_{pc}, E, and Q_{CCD} have a binomial distribution, that is, $\sigma_{Q_{pc}}^{\,2} = Q_{pc}\left(1-Q_{pc}\right)$ and $\sigma_{EQ_{CCD}}^{\,2} = EQ_{CCD}\left(1-EQ_{CCD}\right)$, and G has an exponential distribution ($\sigma_G^{\,2} = G^2$)[25, 26], Eq (2) can be simplified to

$$\sigma_S^{\,2} = \left(2GEQ_{CCD}\right)S \tag{3}$$

Also, because G, E, or Q_{CCD} of an ICCD is typically unknown, Eq. (3) may be rewritten using a single unknown detector parameter as

$$\sigma_S^{\,2} = \alpha_0 S \tag{4}$$

where $\alpha_0 \equiv 2GEQ_{CCD}$. Then, the RSD of stored charge number S becomes

$$\frac{\sigma_S}{S} = \left(\frac{\alpha_0}{S}\right)^{1/2} \tag{5}$$

Note that the number of pixels on a CCD varies with device size; for example, the one used in our experiments had 1024×256 pixels and one column (1×256) of CCD pixels corresponded to one data point (or one wavelength) in the measured spectra. Provided that the spatial distribution profile of the charges on the CCD remains the same during repeated measurements, the RSD of the charge number stored on each CCD column becomes equal to the RSD of the total charge number (S) stored in the whole CCD and thus the RSD of the charge number on column i (S_i) can be written as

$$\frac{\sigma_i}{S_i} = \left(\frac{\alpha_0}{S}\right)^{1/2} \tag{6}$$

Since the line spread function (f) of an ICCD satisfies the following relations

$$f_i = \frac{S_i}{S},\ \sum_i f_i = 1 \tag{7}$$

the variance of S_i becomes

$$\sigma_i^{\,2} = \alpha_0 S f_i^2 \tag{8}$$

When there exist multiple input photon columns as shown in Fig. 2 where each photon column corresponds to the photons from each

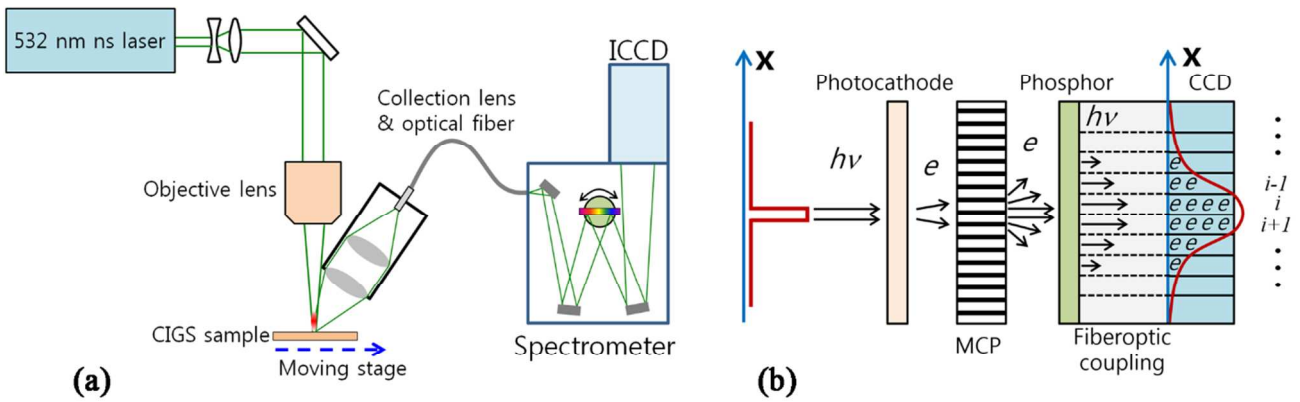

Fig. 1 (a) Schematic diagram of the LIBS setup and (b) the configuration for signal amplification in an ICCD

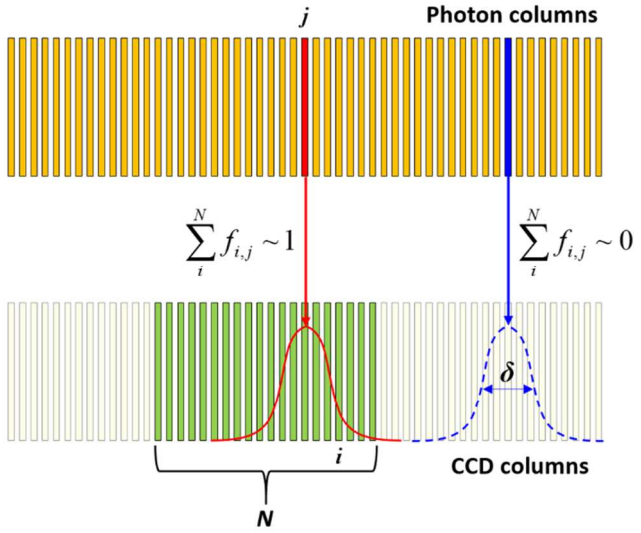

Fig. 2 Dependence of the summation of $f_{i,j}$ on the number of CCD columns and position

wavelength, each photon column contributes with different level to the generation of charge on a CCD column due to spreading. Then, the variance of stored charge number on column i by the j-th input photon column ($S_{i,j}$) can be written similarly as

$$\sigma_{i,j}^{\ 2} = \alpha_0 S f_{i,j}^{\ 2} \text{ with } f_{i,j} = \frac{S_{i,j}}{S} \text{ and } \sum_i f_{i,j} = 1 \qquad (9)$$

and the variance of stored charge number on column i by all input photon columns as

$$\sigma_{i,tot}^{\ 2} = \sum_j \sigma_{i,j}^{\ 2} = \alpha_0 S \sum_j f_{i,j}^{\ 2} \qquad (10)$$

It can be further shown that the variance of total charge on N number of CCD columns by all input photon columns (all j) becomes

$$\sigma_{N,tot}^{\ 2} = \alpha_0 S N \left[\sum_j \left(\sum_i^N f_{i,j} \right)^2 \Big/ N \right] \qquad (11)$$

In the case that the photons from column j fall mostly on the N CCD columns, the function inside the bracket in Eq. (11) becomes equal to unity, whereas that becomes zero if the photons mostly fall on the region outside the N columns (see Fig. 2).

As an example, Fig. 3 shows that the function inside the square bracket in Eq. (11) (denoted by $\boldsymbol{\beta}$) estimated with the Lorentz function approaches unity as $\boldsymbol{n}$ increases, where $\boldsymbol{n}$ is the multiple of the full width at half maximum (δ). Therefore, when the number of CCD columns is sufficiently greater than the full width half maximum of the distribution function ($N >> \delta$), $\boldsymbol{\beta}$ value becomes nearly independent of position and Eq. (11) can be approximated to

$$\sigma_{N,tot}^{\ 2} \approx \alpha_0 S_N \qquad (12)$$

where S_N represents the signal intensity measured with sufficiently large N.

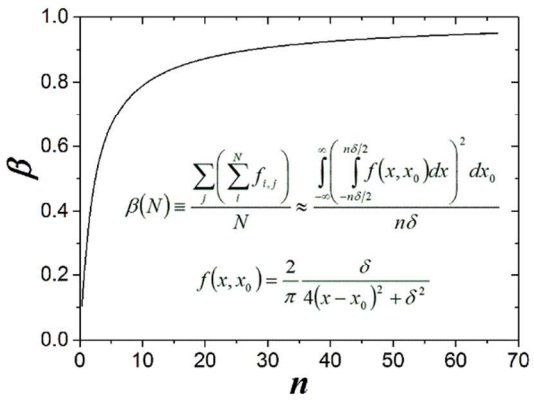

Fig. 3 Integrated distribution function ($\boldsymbol{\beta}$) with respect to CCD column width ($\boldsymbol{n}=N/\delta$) calculated using the Lorentz function

Eq. (12) suggests that when the spectral intensity is measured by integrating the signal over sufficiently large number of CCD columns, an accurate prediction of the detector parameter α_0 can become possible. It should be noted, however, that α_0 can change drastically if only small number of CCD columns are included in the integration (that is, for small $\boldsymbol{n}$ in Fig. 3).

Isolation of plasma fluctuation noise

Since shot noise has the Poisson distribution for which $\sigma_J^2 = J$, the variance of overall photon number incident on the photocathode (σ'^2_J) can be written as a superposition of the shot noise and plasma fluctuation noise components as

$$\sigma'^2_J = J + \sigma_p^2 \qquad (13)$$

where σ_p is the standard deviation of photon number due to shot-to-shot plasma fluctuation alone. By substituting σ_J in Eq. (2) by σ'_J, the variance of overall stored charge on the CCD due to shot noise and plasma fluctuation noise can be represented by

$$\sigma'^{\,2}_S = \left(\frac{\sigma_p}{J} \right)^2 S^2 + \alpha_0 S \qquad (14)$$

From the above equation, the RSD of photon number caused by plasma fluctuation only is obtained by

$$\frac{\sigma_p}{J} = \left[\left(\frac{\sigma'_S}{S} \right)^2 - \frac{\alpha_0}{S} \right]^{1/2} \qquad (15)$$

In LIBS analysis, the ratio of emission intensities rather than absolute intensity is frequently used to reduce the effects of measurement conditions. When $\sigma_1/S_1 \ll 1$ and $\sigma_2/S_2 \ll 1$ are satisfied, the RSD of S_1/S_2 by shot noise becomes equal to the sum of the RSDs of S_1 and S_2 as[27,28]

$$\left. \frac{\sigma_{S_1/S_2}}{S_1/S_2} \right|_{shot} = \left[\frac{\alpha_0}{S_1} + \frac{\alpha_0}{S_2} \right]^{1/2} \qquad (16)$$

Table 1 Spectrometer and ICCD parameters for shot noise measurement

Number	Wavelength range (nm)	Grating (grooves/mm)	Gate width (ms)
I	310 ~ 360	2400	15 ~ 360
II	330 ~ 450	1200	6 ~ 128
III	490 ~ 590	1200	1.5 ~ 32

Then, the RSD component due to plasma fluctuation alone in the measured LIBS signal intensity ratio S_1/S_2 is expressed by subtracting the shot noise component as

$$\left.\frac{\sigma_{S_1/S_2}}{S_1/S_2}\right|_{plasma} = \left[\left(\left.\frac{\sigma_{S_1/S_2}}{S_1/S_2}\right|_{m}\right)^2 - \frac{\alpha_0}{S_1} - \frac{\alpha_0}{S_2}\right]^{1/2} \quad (17)$$

Experiments

Measurement of detector shot noise

For the estimation of detector shot noise, an intensity calibrated deuterium-halogen light source (AvaLight-DH-CAL, Avantes Inc., wavelength 200 nm~1099 nm, Max. Drift ±0.5%/hr) was coupled to the collection lens side end of the optical fiber bundle in Fig. 1(a). Then, intensity measurement was carried out over three different wavelength regimes of interest. The spectrometer and ICCD parameters such as MCP gain, grating density, wavelength range, slit width, etc. for shot noise estimation were set to the same values as those for LIBS measurement. Table 1 shows the grating density and gate width for each wavelength regime. To evaluate the detector parameter (α_0) in Eq. (12), gate width was varied over a wide range as a way to change signal intensity. For each gate width condition, signal intensity was measured fifty times from which the average intensity and standard deviation were estimated. Drift in the successively measured intensity data was subtracted after a second order polynomial fitting.

Spectral line selection

Table 2 shows the properties of spectral lines selected for plasma RSD estimation from the LIBS spectra of CIGS film, lying within the three wavelength regimes of interest. These spectral lines were carefully selected based on our earlier study[1,2,29,30]. Specifically, the intensity ratios of Cu 324.7 nm to In 325.6 nm and Ga 417.2 nm to In 410.2 nm were known to be little influenced by measurement conditions[1,29]. The Cu lines (510.6 and 515.3 nm) were for depth profiling of CIGS thin film[30] which also have been often used for estimation of plasma temperature[29,31-33]. Fig. 4 shows an example of these selected spectral lines measured during LIBS analysis of CIGS thin film.

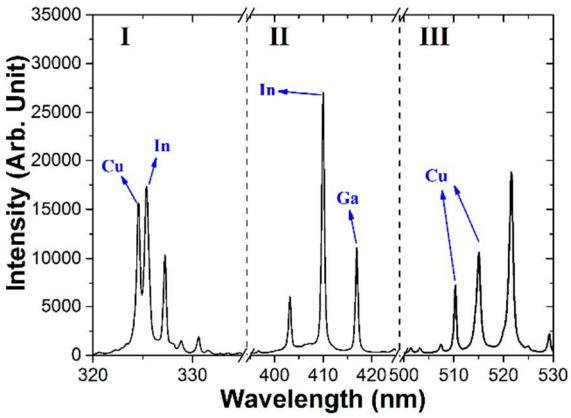

Fig. 4 The spectral lines of the three wavelength regimes measured in LIBS analysis of a CIGS thin film

LIBS measurement

The CIGS thin film layer of a commercial CIGS solar cell module fabricated on glass substrate by sputtering was used as the LIBS measurement sample (5 cm × 5 cm). To directly ablate the CIGS layer, the transparent conducting oxide and buffer layers on top of the CIGS film were removed by etching in a dilute hydrochloric acid solution.

For LIBS analysis, the CIGS thin film sample was irradiated by a scanning laser beam (Nd:YAG laser, 532 nm, 5 ns, 5 Hz, top-hat profile) at the velocity of 0.75 mm/s. The ablation was carried out with two different laser spot diameters of 42 and 104 μm and varying laser pulse energy (0.16 ~ 2.9 mJ). The pulse-to-pulse variation of laser energy was verified to be less than 2% using a laser energy meter (PE25BF-DIF-C, NOVA II meter, Newport) and little drift was observed. For the analysis of RSD, LIBS spectra were successively collected from 114 points (38 points × 3 scan, spot-to-spot separation=150 μm). Again, the drift in signal intensity and intensity ratio was subtracted after a second order polynomial fitting. The possible change of RSD due to signal drift was estimated to be less than 2%.

For the ICCD detector (PI-MAX3, Princeton Instruments), MCP gain was set to a fixed value of 5% during the measurements and gate delay was varied from 120 ns to 3600 ns at which the emission almost completely disappeared. Gate widths were adjusted to the values in Table 2 so that either the detector did not become saturated at short gate delay conditions

Table 2. Spectral lines selected for RSD analysis [34, 35]

Wavelength regime	Gate width	Element	Wavelength (nm)	E_i (eV)	E_k (eV)	A_{ki}	g_i	g_k	$A_{ki}g_k$	Ionization energy (eV)
I	50 ns, 100 ns	Cu I	324.754	0.000	3.817	1.395E8	2	4	5.58E8	7.73
		In I	325.608	0.274	4.081	1.30E8	4	6	7.80E8	5.79
II	40 ns, 80 ns	In I	410.175	0.000	3.022	5.00E7	2	2	1.00E8	5.79
		Ga I	417.204	0.102	3.073	9.45E7	4	2	1.89E8	6.00
III	150 ns, 300 ns	Cu I	510.554	1.389	3.817	2.00E6	6	4	8.00E6	7.73
		Cu I	515.324	3.786	6.191	6.00E7	2	4	2.40E8	7.73

or sufficiently high spectral intensity could be achieved at long gate delay conditions (>800 ns). Since the photon fluence of the deuterium-halogen light source used for the determination of shot noise coefficient (α_0) was significantly lower than that of the LIBS plasma, it was checked and verified using neutral density filters that the detector signal was linearly increasing with respect to photon fluence, up to the highest photon fluence condition of current experiments, which confirmed the validity of α_0 estimated with the deuterium-halogen light source for the shot noise analysis of LIBS plasma. The ICCD detector was triggered by the Q-switch signal of the laser. The gating jitter of the ICCD provided by the manufacturer was 35 ps and the jitter of the laser (Polaris II, New Wave Research) was ±1 ns. It seemed that the contribution to RSDs of the jitters was negligible.

Results and discussion

Estimation of detector noise parameter (α_0)

To determine the detector shot noise parameter α_0 in Eq. (12), intensity of the calibration light source was measured over wide ranges of gate width and integration width. Fig. 5(a) shows the spectra for varying gate widths over the wavelength regime III. Since α_0 approaches a stationary value as N increases, the variation of α_0 with respect to N was examined by increasing the integration width around the spectral line of interest, e.g., the width by red vertical solid lines around 515.3 nm in Fig. 5(a). For each gate width and integration width, the intensity of calibration light source was measured repeatedly and then drift correction was made as shown in Fig. 5(b). Fig. 5(c) shows the measured variance with respect to signal intensity in log scale. The data points were well fitted into straight lines with the slope of 1/2, which confirms that the variance is linearly proportional to intensity as predicted by Eq. (12) regardless of integration width. From the linear fitting of variance data with intensity, the detector parameter α at varying integration width was determined. As the integration width increases, α approaches a stationary value (α_0) as shown in Fig. 5(d) which shows nearly the same trend as that in Fig. 3 predicted with the Lorentz function. The α_0 values for the wavelength regimes I and II were estimated similarly. The α_0 values for all three regimes were determined to be 16.8, 13.9 and 15.4 for the regime I, II and III, respectively. The difference in α_0 values between wavelength regimes could be due to the non-uniformity of MCP gain (G) or the quantum efficiency (E or Q_{CCD}) of phosphor and/or CCD[36].

RSD of LIBS signal intensity

Fig. 6 shows the RSD (after drift correction) of absolute intensity of the spectral lines in Table 2 over wide range of spectral line intensity and two different laser spot diameters (42 μm and 104 μm). The intensity of each data point was

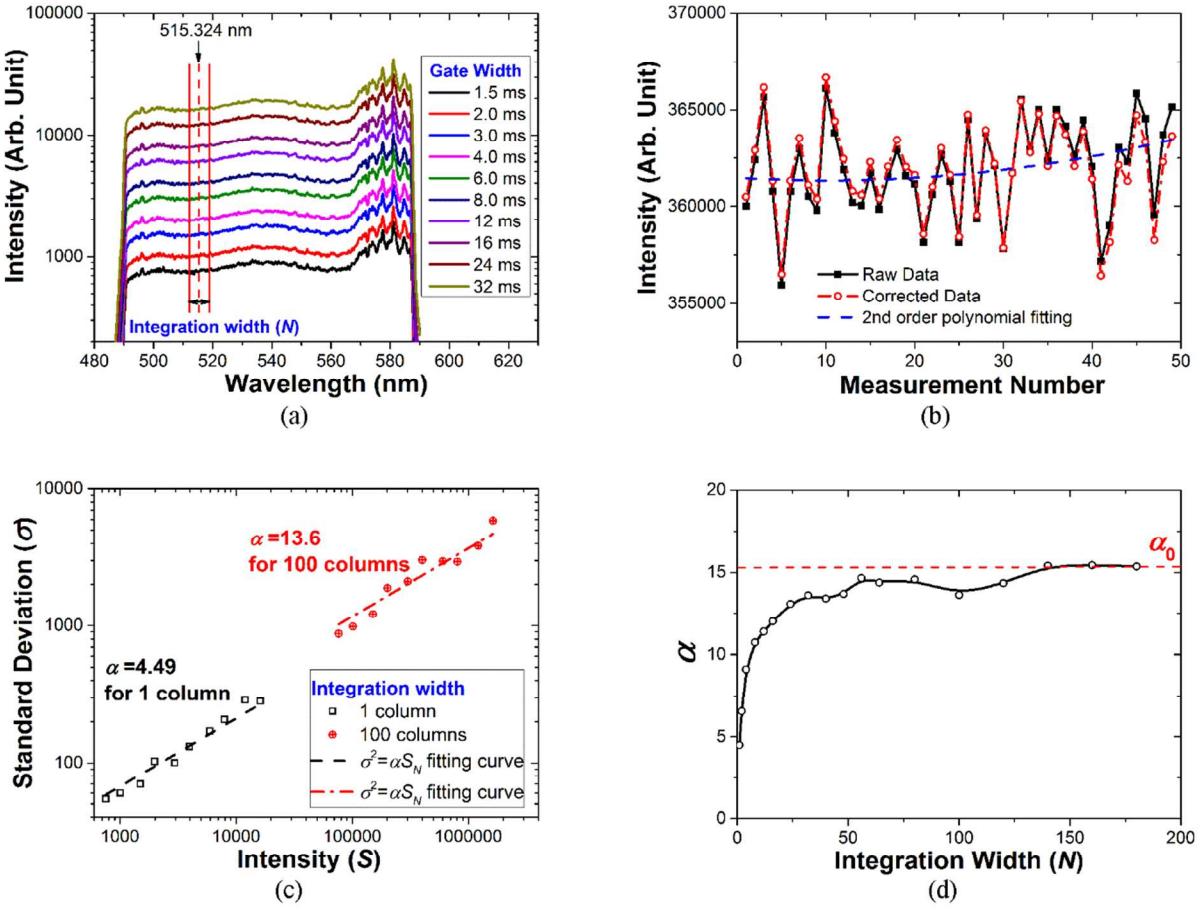

Fig. 5 (a) Spectra of the calibration light source in the wavelength regime III, (b) drift correction of the measured spectral intensities (50 measurements), (c) determination of detector parameters for different integration widths and (d) the variation of detector parameter with respect to integration width.

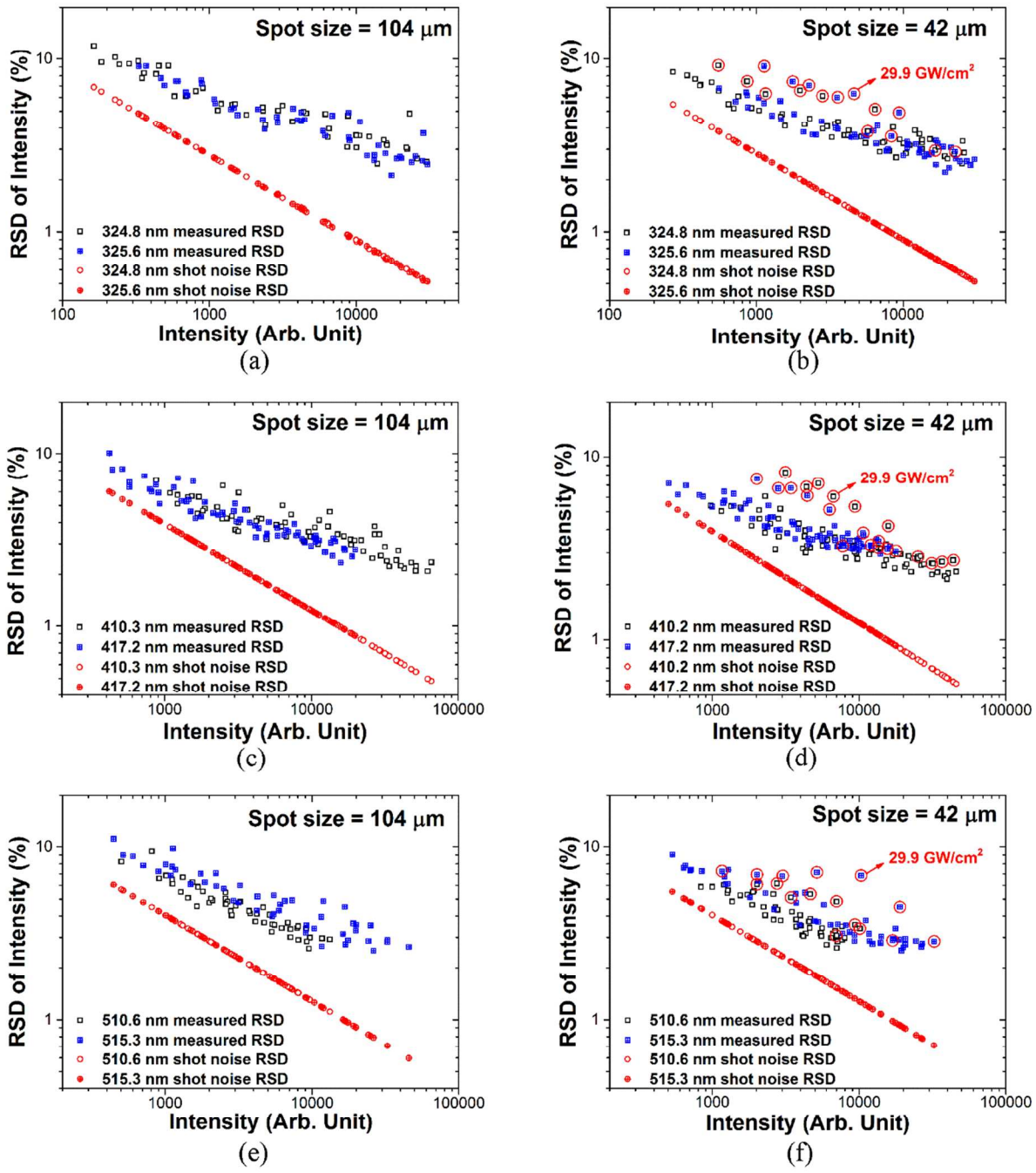

Fig. 6 The measured RSD and shot noise RSD of the intensities of six spectral lines at two spot size conditions (42 μm and 104 μm)

determined by varying laser energy and/or gate delay. The RSD of detector shot noise was calculated by Eq. (5) by using the α_0 values obtained above. Note that the difference between the measured RSD and shot noise RSD represents the RSD by plasma fluctuation. As the signal intensity decreases, detector shot noise increases and the difference is reduced, implying that detector noise becomes increasingly significant for low intensity LIBS measurement. In general, the tendency of RSD variation with respect to signal intensity remained similar between different spot diameter conditions and spectral lines. A further detailed inspection of the RSD, however, revealed that RSD values were greater at the highest laser irradiance condition (29.9 GW/cm^2) of this study for the smaller spot diameter (42 μm). The reason for the increase of RSD at high laser irradiance for small spot diameter condition needs further investigation.

Fig. 7 shows the behavior of RSD of the absolute intensity due to plasma fluctuation alone for varying laser irradiance and gate delay conditions. It is observed that the RSD by plasma fluctuation starts increasing as the laser irradiance drops below a certain level, for example, 1.26 GW/cm^2 in the present experiments. Also, the RSD by plasma fluctuation tended to increase for increasing gate delay. This behavior of RSD by plasma fluctuation may be associated with the ablation and temperature characteristics as follow.

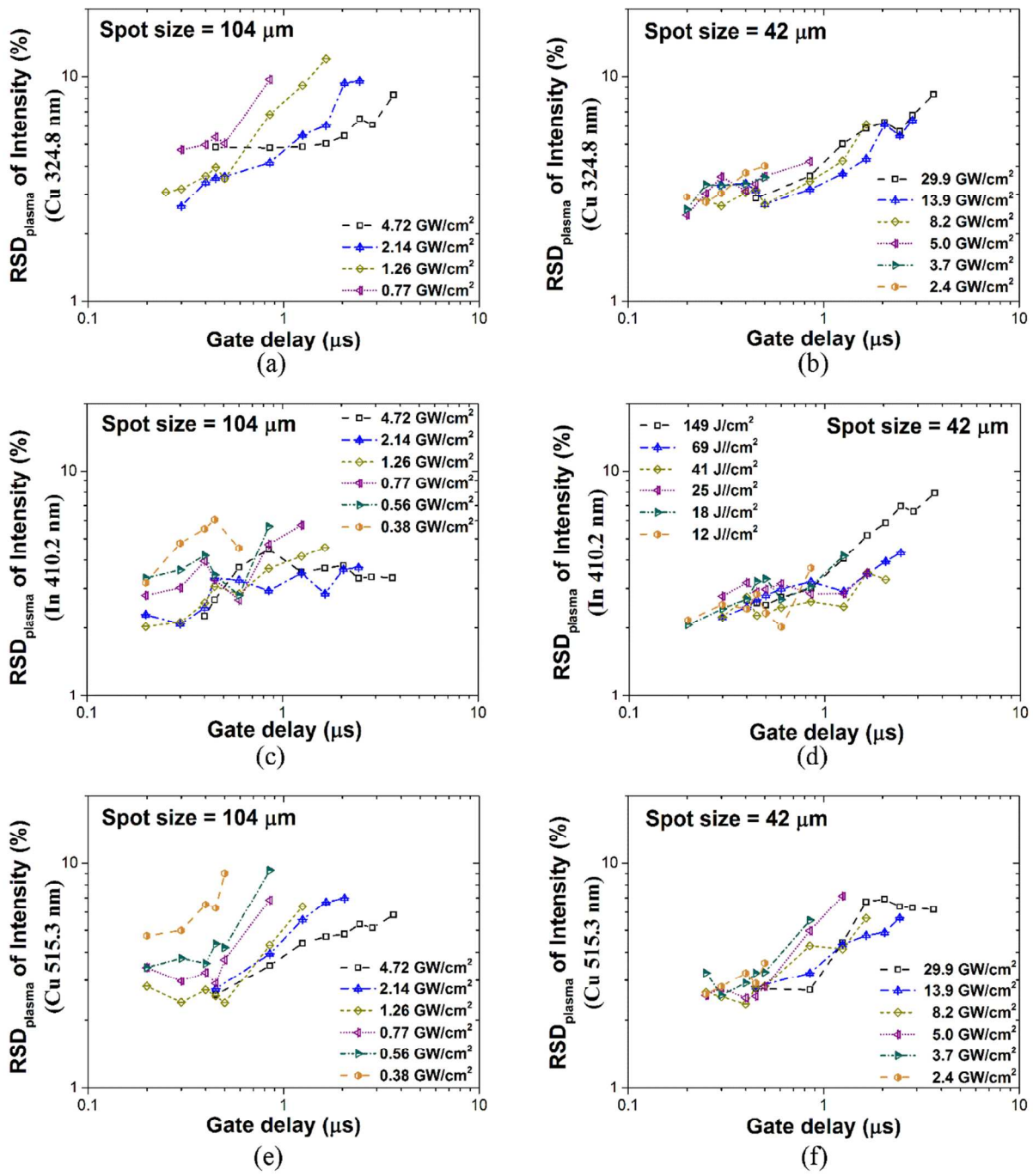

Fig. 7 The RSD by plasma fluctuation of the intensities of three spectral lines at two spot size conditions (42 μm and 104 μm)

It can be shown that the relative variation of spectral line intensity due to plasma fluctuation is expressed by (see Appendix A for details)

$$\frac{\Delta J^S}{J^S} = \left[\frac{E_k - \langle E^S \rangle}{k_B T}\right]\frac{\Delta T}{T} + {}^{II}W^S \frac{\Delta n_e}{n_e} + \frac{\Delta\left(n^S V\right)}{n^S V} \qquad (18)$$

where J^S is the spectral intensity of an atomic line represented by the Boltzmann equation[37]

$$J^S = \frac{hc}{4\pi\lambda_{ki}} A_{ki} \times \frac{g_k \exp\left(-E_k/k_B T\right) {}^{I}W^S}{{}^{I}U^S(T)} \times n^S V \qquad (19)$$

where h is the Planck constant (6.626×10^{-34} m^2kg/s), c is the speed of light (2.998×10^8 m/s), λ_{ki} is the wavelength of the light emitted by atomic transition from state k to state i, A_{ki} is transition probability, n^S is total atom number density (neutral atoms+ions), ${}^{I}W^S$ is the ratio of neutral atom to total atom densities, g_k and E_k are the statistical weight and energy level of state k, respectively, k_B is the Boltzmann constant (1.381×10^{-23} J/K), T is plasma temperature, ${}^{I}U^S$ is a partition function of neutral atoms, V is plasma volume, n_e is plasma

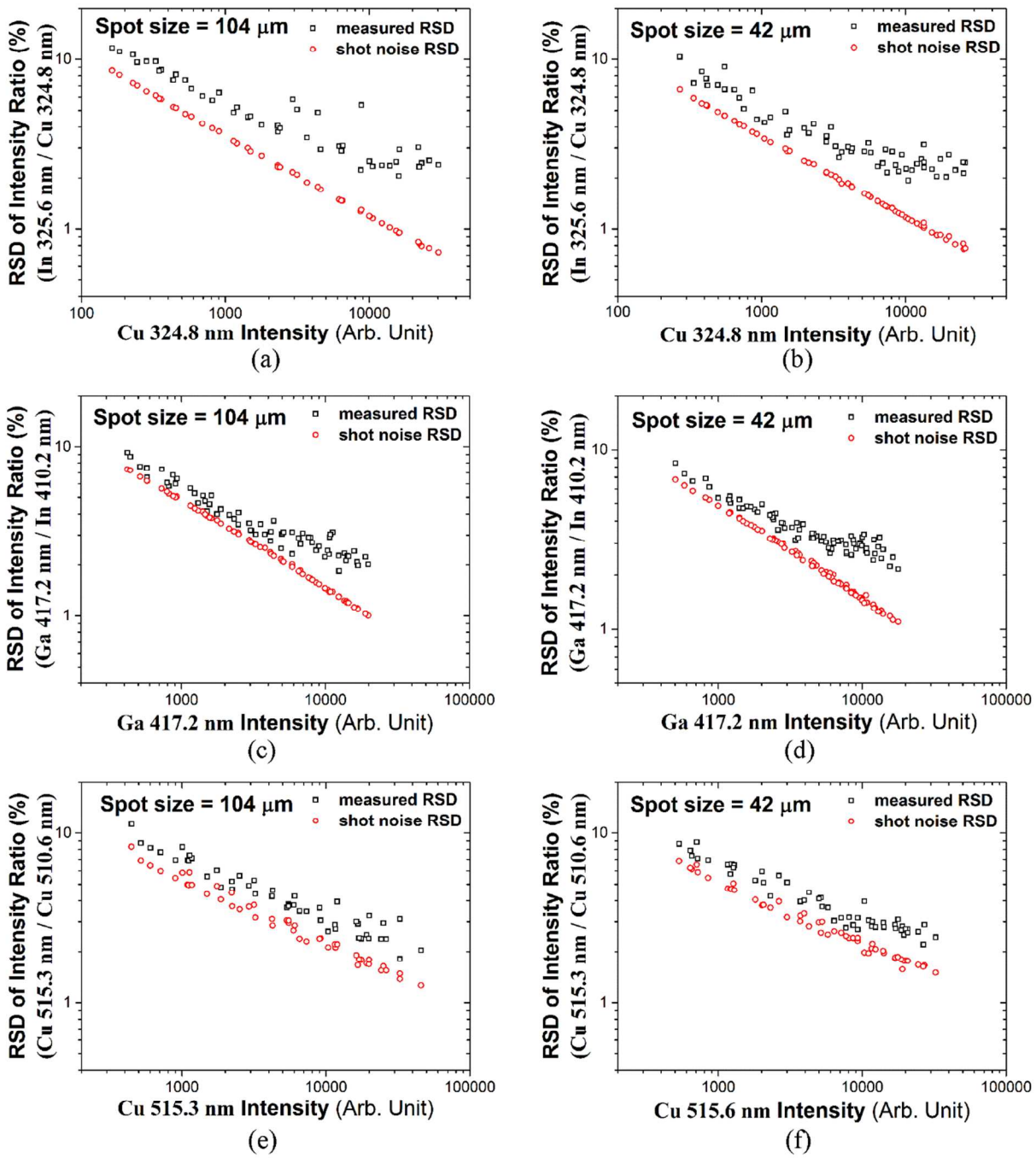

Fig. 8 The measured RSD and shot noise RSD of the intensity ratios of three spectral line pairs at two spot size conditions (42 μm and 104 μm)

density, ${}^{II}W^{S}$ is the ratio of singly ionized atoms, superscript S represents a species, and

$$\left\langle E^{S}\right\rangle \equiv {}^{I}W^{S}\left\langle {}^{I}E^{S}_{exc}\right\rangle + {}^{II}W^{S}\left[\left\langle {}^{II}E^{S}_{exc}\right\rangle + \frac{3}{2}k_{B}T + E^{S}_{ion}\right] \quad (20)$$

with

$$\left\langle {}^{Z}E^{S}_{exc}\right\rangle = \frac{\sum_{k} {}^{Z}E_{k}g_{k}\exp\left(-{}^{Z}E_{k}/k_{B}T\right)}{{}^{Z}U^{S}(T)} \quad \text{and } Z=I \text{ or } II$$

where the superscripts I and II stand for neutral atom and singly ionized atom, respectively, and $E_{ion}{}^{S}$ is the first ionization energy of species S, $\langle {}^{Z}E^{S}_{exc}\rangle$ is the average excitation energy of a single atom of species S at ionization state Z in the plasma. The first term of Eq. (20) is the product of the neutral atom fraction and the average excitation energy per neutral atom. The second term is the product of ion fraction and the average energy of an ion which is represented by the terms inside the bracket as the sum of average excitation energy of singly ionized atom, kinetic energy of electron, and first ionization

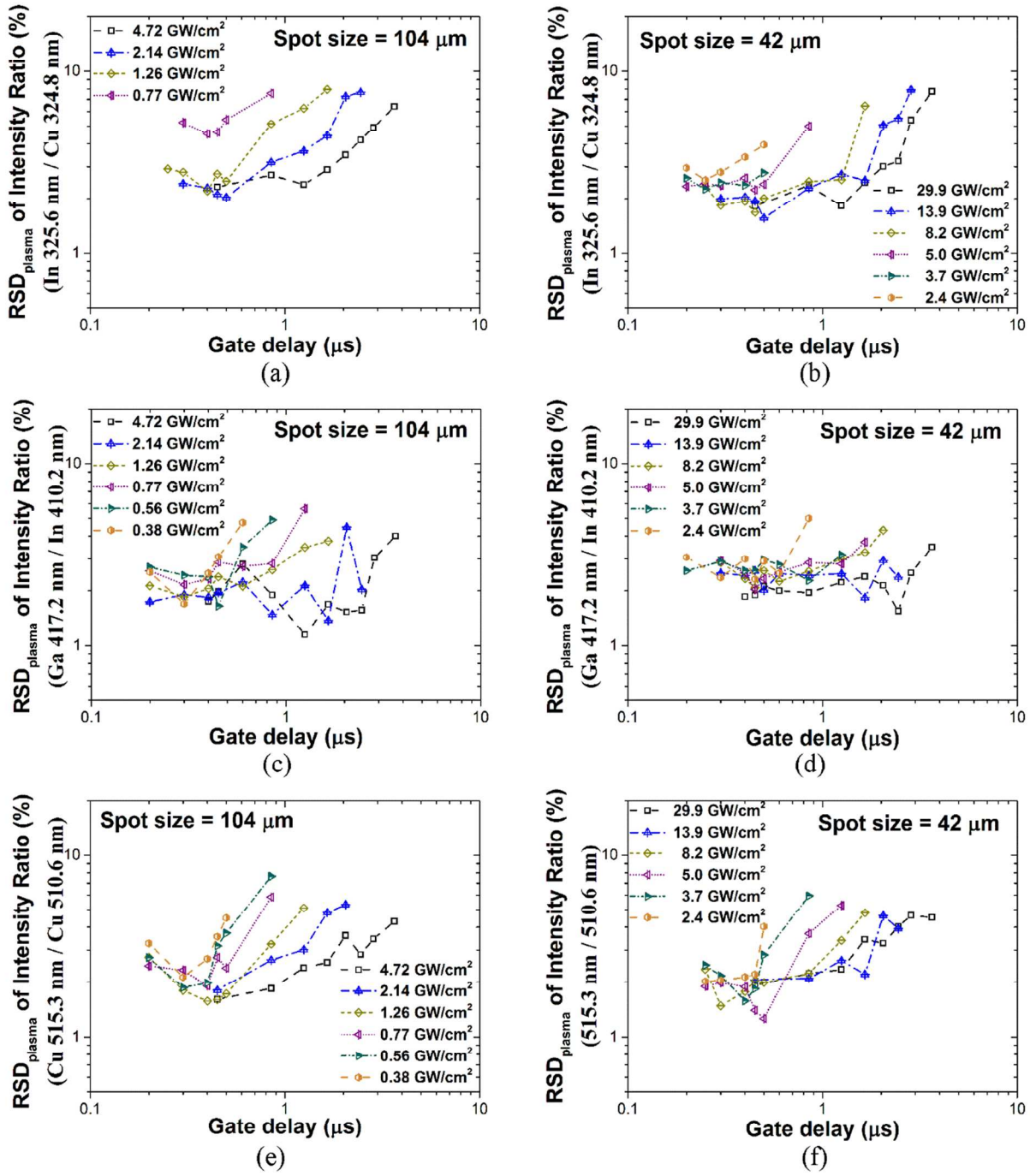

Fig. 9 The RSD by plasma fluctuation of the intensity ratios of three spectral line pairs at two spot size conditions (42 μm and 104 μm)

energy. In short, $<E^S>$ represents the average energy that a single atom possesses in the plasma satisfying local thermodynamic equilibrium (LTE) condition, excluding the kinetic energy of the atom itself.

Note that the first term on the right hand side of Eq. (18) represents the contribution of plasma temperature fluctuation to the RSD of spectral line intensity. Because the value of $\langle E^S \rangle$ increases with plasma temperature, the coefficient of the first term ($\left(E_k - \langle E^S \rangle\right)/k_B T$) increases for decreasing plasma temperature. The second and third terms of Eq. (18) represent the contributions of plasma density fluctuation and the fluctuation in ablation mass ($n^S V$), respectively. When the laser irradiance is close to ablation threshold, the variation of ablated mass will become greater, leading to the observed increase in plasma-fluctuation-induced RSD at low laser irradiance. As the gate delay increases, the coefficient of the first term increases due to temperature decrease, again leading to an increase of plasma-fluctuation-induced RSD as observed in Fig. 7. Eq. (18) also predicts that the RSD due to plasma fluctuation increases with upper level energy. In fact, it was shown that the RSDs of Cu 515.3 nm line with a higher upper level energy

(E_k=6.191 eV) was greater than that of Cu 510.6 nm line (E_k=3.817 eV) as shown in Figs. 6(e) and 6(f). Note that self-absorption was assumed to be negligible in Eq. (18). However, the spectral lines in Table 2, except Cu 510.6 and 515.3 nm, are expected to be highly self-absorbing due to their low lower level energy, high transition probability, and the high elemental concentrations of In (~17 at%), Ga (~8 at%) and Cu (~25 at%). It can be shown that the RSD of highly self-absorbing plasma can be represented by a similar expression with the consideration of optical depth (see Appendix B for details).

RSD of LIBS signal intensity ratio

Fig. 8 shows the RSD of intensity ratio between the selected spectral lines in each wavelength regime with respect to signal intensity. For these intensity ratio data, it is clear that the difference between the RSD values of measured LIBS data and those of shot noise decreased significantly as compared with that of absolute intensity in Fig. 6. These results confirm that the influence of plasma fluctuation can be reduced in LIBS analysis by using intensity ratio rather than absolute intensity. Especially, it is noteworthy that the measured RSD of the intensity ratio of Ga 417.2 nm to In 410.3 nm became nearly the same as the shot noise RSD as the signal intensity decreased, whereas the measured RSD of other pairs of spectral lines had a finite difference from shot noise RSD even at low intensity. The plasma-fluctuation-induced RSD of intensity ratio in Fig. 9, calculated by Eq. (17), also showed that the RSD of Ga 417.2 nm / In 410.2 nm intensity ratio, especially Fig. 9(d), remained nearly constant for all gate delay conditions while the RSD of other line pairs in Figs. 9(a), 9(b), 9(e) and 9(f) was continuously changing. This difference in RSD behavior of LIBS signal intensity ratio between spectral line pairs is understood to be related to the spectral line properties of the elements as discussed below.

For the intensity ratio of two spectral lines of different species A and B, denoted by $\eta \equiv J_B/J_A$, the relative variation of η can be written by using Eq. (18) as

$$\begin{aligned}\frac{\Delta\eta}{\eta} &= \frac{\Delta J^B}{J^B} - \frac{\Delta J^A}{J^A} \\ &= \left[\frac{E_k^B - E_k^A}{k_B T} - \frac{\langle E^B\rangle - \langle E^A\rangle}{k_B T}\right]\frac{\Delta T}{T} \\ &\quad + \left({}^{II}W^B - {}^{II}W^A\right)\frac{\Delta n_e}{n_e} + \frac{\Delta\left(n^B/n^A\right)}{n^B/n^A}\end{aligned} \qquad (21)$$

Each term on the right hand side of Eq. (21) corresponds to the contribution by fluctuation in plasma temperature, plasma density and the density ratio of ablated mass, respectively. The first term for plasma temperature decreases if both the upper level energies of the spectral lines and the ionization energies of the elements are similar. The second term decreases if the ionization energies are similar. The different RSD behavior of Ga 417.2 nm / In 410.2 nm intensity ratio in Fig. 9(d) from those in Figs. 9(b) and 9(f) is due to the similarity in upper level energies of the selected spectral lines ($E_{k,Ga\ 417.2\ nm}$=3.07 eV and $E_{k,In\ 410.2\ nm}$=3.02 eV) and in ionization energies of the elements ($E_{ion,Ga}$=6.00 eV and $E_{ion,In}$=5.79 eV). The third term for ablated mass in Eq. (21) is represented by density ratio of the elements (n^B/n^A), whereas the corresponding term in Eq. (18) for absolute intensity includes ablated mass ($n^S V$). Since the ratio of ablated mass between elements remains much consistent than the absolute mass for varying laser fluence, it is expected that the RSD of intensity ratio is less influenced by lowering the laser fluence. Again, self-absorption was ignored in Eq. (21), and the equation for highly self-absorbing lines is shown in the Appendix B.

In addition, Fig. 9 shows that unlike the absolute intensity case, the plasma-fluctuation-induced RSD of intensity ratio in Figs. 9(a), 9(b), 9(e) and 9(f) decreased initially to a minimum value for increasing gate delay and then started increasing rapidly at longer gate delay conditions. This result indicates that the behavior of plasma-fluctuation-induced RSD of intensity ratio is not the same as that of absolute intensity which increases monotonically with gate delay.

The results for LIBS signal intensity ratio in Figs. 8 and 9 demonstrate that to minimize plasma-fluctuation-induced RSD the line pairs needs to be carefully selected considering their spectral properties and the optimal gate delay may be determined at a slightly longer value than the possible shortest gate delay in experiments.

Conclusions

To investigate the influence of signal intensity and measurement parameters on the precision of LIBS analysis, the contribution of shot-to-shot fluctuation of laser plasma to the RSD was quantitatively estimated by subtracting the detector shot noise portion from the overall RSD of the measured LIBS signal intensity or intensity ratio. It was demonstrated that the detector noise can be represented by a linear relation to signal intensity and the proportionality coefficient can be determined experimentally. Using the analysis of LIBS spectra obtained with CIGS thin film sample over widely varying laser irradiance and gate delay conditions as well as two different spot diameters, it was (i) confirmed that the magnitude of plasma-fluctuation-induced RSD of absolute intensity is greater than that of intensity ratio and (ii) found that the plasma-fluctuation-induced RSD of intensity ratio initially decreases and then increases with gate delay, whereas that of absolute intensity increases monotonically. It was further shown that the plasma-fluctuation-induced RSD of intensity ratio can be nearly independent of gate delay or laser irradiance for properly selected spectral line pairs. It is expected that the proposed approach for separate analysis of detector and plasma fluctuation RSDs could be useful to understand the influence of individual measurement parameter on the precision during LIBS analysis.

Acknowledgements

This work was supported by National Research Foundation of Korea (NRF) grant funded by Korea government (MEST) (No. 2014049289)

Appendix A: Derivation of Eq. (18)

For optically thin and spatially uniform plasma with a volume V, the spectral intensity of an atomic line is expressed by the Boltzmann equation as[37]

$$J^S = \frac{hc}{4\pi\lambda_{ki}} A_{ki} \times \frac{g_k \exp\left(-E_k/k_B T\right)}{{}^I U^S(T)} \times {}^I W^S \times n^S V \qquad (A1)$$

The relative variation of line intensity can then be derived to

$$\frac{\Delta J^S}{J^S} = \Delta\left[\frac{g_k \exp(-E_k/k_BT)}{{}^I U^S(T)}\right] \Big/ \left[\frac{g_k \exp(-E_k/k_BT)}{{}^I U^S(T)}\right] + \frac{\Delta {}^I W^S}{{}^I W^S} + \frac{\Delta(n^S V)}{n^S V} \quad \text{(A2)}$$

In Eq. (A2), the first term on the right hand side (RHS) is a function of plasma temperature only. The numerator of the first term can be rewritten as

$$\Delta\left[\frac{g_k \exp(-E_k/k_BT)}{{}^I U^S(T)}\right] = \left[\frac{E_k}{k_BT} - \frac{T}{{}^I U^S(T)}\frac{d\,{}^I U^S(T)}{dT}\right]\frac{\Delta T}{T} \times \frac{g_k \exp(-E_k/k_BT)}{{}^I U^S(T)} \quad \text{(A3)}$$

By the definition of partition function, the second term inside the square bracket on the RHS of Eq. (A3) becomes

$${}^I U^S = \sum_k g_k \exp(-E_k/k_BT) \quad \text{(A4)}$$

$$\frac{T}{{}^I U^S(T)}\frac{d\,{}^I U^S(T)}{dT} = \frac{\sum_k E_k g_k \exp(-E_k/k_BT)}{{}^I U^S(T)}\frac{1}{k_BT} \equiv \frac{\langle {}^I E^S_{exc}\rangle}{k_BT} \quad \text{(A5)}$$

where $\langle {}^I E^S_{exc}\rangle$ is the average excitation energy of neutral atom of species S in plasma. By using Eq. (A3) and (A5), the first term on the RHS of Eq. (A2) is simplified to

$$\Delta\left[\frac{g_k \exp(-E_k/k_BT)}{{}^I U^S(T)}\right] \Big/ \left[\frac{g_k \exp(-E_k/k_BT)}{{}^I U^S(T)}\right] = \frac{E_k - \langle {}^I E^S_{exc}\rangle}{k_BT}\frac{\Delta T}{T} \quad \text{(A6)}$$

Provided that LTE condition is satisfied in the plasma, the relation between the ionic species density and neutral species density follows the Saha equation[37] as

$$n_e \frac{{}^{II} n^S}{{}^I n^S} = \frac{(2\pi m_e k_B T)^{3/2}}{h^3}\frac{2\,{}^{II} U^S(T)}{{}^I U^S(T)} \exp\left(-\frac{E^S_{ion}}{k_BT}\right) \quad \text{(A7)}$$

where m_e is electron mass, ${}^I n^S$ is neutral species density and ${}^{II} n^S$ is ionic species density. If the second and higher order ionizations are negligible and the ratio of ionic species density to neutral species density, denoted by $X(n_e,T)$, can be written as

$$X(n_e,T) \equiv \frac{{}^{II} n^S}{{}^I n^S} = \frac{2(2\pi m_e k_B)^{3/2}}{n_e h^3} \times \frac{{}^{II} U^S(T) T^{3/2} \exp(-E^S_{ion}/k_BT)}{{}^I U^S(T)} \equiv R(n_e) Q(T) \quad \text{(A8)}$$

and the fraction of neutral species as

$${}^I W^S = \frac{{}^I n^S}{{}^I n^S + {}^{II} n^S} = \frac{1}{1+X} \quad \text{(A9)}$$

Using Eq. (A9), the second term of Eq. (A2) can be rewritten as

$$\frac{\Delta {}^I W^S}{{}^I W^S} = -\frac{1}{1+X}\Delta X = -{}^{II} W^S\left(\frac{T}{Q}\frac{dQ}{dT}\frac{\Delta T}{T} + \frac{n_e}{R}\frac{dR}{dn_e}\frac{\Delta n_e}{n_e}\right) \quad \text{(A10)}$$

Since

$$\frac{dQ}{dT} = \left(\frac{\langle {}^{II} E^S_{exc}\rangle - \langle {}^I E^S_{exc}\rangle + 3k_BT/2 + E^S_{ion}}{k_BT}\right)\frac{Q}{T} \quad \text{(A11)}$$

and

$$\frac{dR}{dn_e} = -\frac{2(2\pi m_e k_B)^{3/2}}{n_e^2 h^3} = -\frac{R}{n_e} \quad \text{(A12)}$$

Eq. (A10) can be rewritten to

$$\frac{\Delta {}^I W^S}{{}^I W^S} = -{}^{II} W^S\left[\frac{\langle {}^{II} E^S_{exc}\rangle - \langle {}^I E^S_{exc}\rangle + 3k_BT/2 + E^S_{ion}}{k_BT}\frac{\Delta T}{T} - \frac{\Delta n_e}{n_e}\right] \quad \text{(A13)}$$

By substituting Eqs. (A6) and (A13), Eq. (A2) is rewritten as

$$\frac{\Delta J^S}{J^S} = \frac{E_k - \langle E^S\rangle}{k_BT}\frac{\Delta T}{T} + {}^{II} W^S\frac{\Delta n_e}{n_e} + \frac{\Delta(n^S V)}{n^S V} \quad \text{(A14)}$$

$$\langle E^S\rangle \equiv {}^I W^S \langle {}^I E^S_{exc}\rangle + {}^{II} W^S\left[\langle {}^{II} E^S_{exc}\rangle + \frac{3}{2}k_BT + E^S_{ion}\right] \quad \text{(A14a)}$$

$$\langle {}^Z E^S_{exc}\rangle = \frac{\sum_k {}^Z E_k g_k \exp(-{}^Z E_k/k_BT)}{{}^Z U^S(T)} \quad \text{(A14b)}$$

Appendix B: Equations for highly self-absorbing lines

The intensity of a highly self-absorbing line (J'^S) can be written by[38, 39]

$$J'^S = J^S\left[\frac{1-\exp(-\tau^S)}{\tau^S}\right]^{0.46} \quad \text{(B1)}$$

where J^S is the intensity of optically thin plasma in Eq. (A1) and τ^S is optical depth[38, 39]. When the photon energy is much greater than the plasma temperature (i.e. $\exp[-(E_k-E_i)/kT] \ll 1$) and Stark broadening is dominant and proportional to plasma density, τ^S can be written as[38, 39]

$$\tau^S \approx \frac{\lambda^4}{8\pi c} A_{ki} \frac{g_k}{g_i} \frac{2}{\pi} \times \frac{g_i \exp\left(-E_i/kT\right)_I W^S \times n^S V \times \frac{n_{e0}}{S_0 n_e w_{ki}}}{{}^I U^S(T)} \quad \text{(B2)}$$

where c is the speed of light, E_i is the lower level energy, S_0 is the characteristic area of the plasma (V=$S_0 l$, l is the characteristic plasma length), n_{e0} is the reference plasma density and w_{ki} is the electron impact width at the reference plasma density. When τ^S >>1 (i.e. exp(-τ^S) ≈ 0), Eq. (B1) can be approximated to

$$J'^S \approx J^S \left[\frac{1}{\tau^S}\right]^{0.46} \quad \text{(B3)}$$

Thus, the relative variation of intensity of a highly self-absorbing line (J'^S) can be modified into

$$\frac{\Delta J'^S}{J'^S} = \frac{\Delta J^S}{J^S} - 0.46 \frac{\Delta \tau^S}{\tau^S} \quad \text{(B4)}$$

Similarly to those in Appendix A, $\Delta\tau^S/\tau^S$ can be simplified to

$$\frac{\Delta \tau^S}{\tau^S} = \left[\frac{E_i - \langle E^S \rangle}{k_B T}\right] \frac{\Delta T}{T} + \left({}^{II}W^S - 1\right) \frac{\Delta n_e}{n_e} + \frac{\Delta\left(n^S V\right)}{n^S V} - \frac{\Delta S_0}{S_0} \quad \text{(B5)}$$

From (B4) and (B5), the relative variation of the intensity of a highly self-absorbing line is written by

$$\begin{aligned} \frac{\Delta J'^S}{J'^S} = & \left[\frac{E_k - 0.46E_i - 0.54\langle E^S \rangle}{k_B T}\right] \frac{\Delta T}{T} \\ & + \left[0.46 + 0.54\,{}^{II}W^S\right] \frac{\Delta n_e}{n_e} \\ & + \frac{\Delta\left(n^S V\right)}{n^S V} - 0.46 \frac{\Delta\left(n^S l\right)}{n^S l} \end{aligned} \quad \text{(B6)}$$

For the intensity ratio of two spectral lines of different species A and B, denoted by $\eta \equiv J_B/J_A$, the relative variation of η can be written by using Eq. (B6) as

$$\begin{aligned} \frac{\Delta \eta'}{\eta'} = & \left[\frac{E_k^B - E_k^A - 0.46\left(E_i^B - E_i^A\right)}{k_B T} - 0.54 \frac{\langle E^B \rangle - \langle E^A \rangle}{k_B T}\right] \frac{\Delta T}{T} \\ & + 0.54\left({}^{II}W^B - {}^{II}W^A\right) \frac{\Delta n_e}{n_e} + 0.54 \frac{\Delta\left(n^B/n^A\right)}{n^B/n^A} \end{aligned} \quad \text{(B7)}$$

Notes and references

1 Jung-Hwan In, Chan-Kyu Kim, Seok-Hee Lee, Hee-Sang Shim, Sungho Jeong, *J. Anal. At. Spectrom.*, 2013, **28**, 890-900.

2 Jung-Hwan In, Chan-Kyu Kim, Seok-Hee Lee, Sungho Jeong, *J. Anal. At. Spectrom.*, 2013, **28**, 473-481.

3 J. Gurell, A. Bengtson, M. Falkenstrom, B.A.M. Hansson, *Spectrochim. Acta Part B*, 2012, **74-75**, 46-50.

4 P. Werheit, C. Fricke-Begemann, M. Gesing, R. Noll, *J. Anal. At. Spectrom.*, 2011, **26**, 2166-2174.

5 R. Noll, C. Fricke-Begemann, M. Brunk, S. Connemann, C. Meinhardt, M. Scharun, V. Sturm, J. Makowe, C. Gehlen, *Spectrochim. Acta Part B*, 2014, **93**, 41-51.

6 V. Sturm, R. Fleige, M. De Kanter, R. Leitner, K. Pilz, D. Fischer, G. Hubmer, R. Noll, *Anal. Chem.*, 2014, **86**, 9687-9692.

7 M. Gaft, E. Dvir, H. Modiano, U. Schone, *Spectrochim. Acta Part B*, 2008, **63**, 1177-1182.

8 W. Yin, L. Dong, W. Ma, S. Jia, *Appl. Spectrocs.*, 2009, **63**(8), 865-872.

9 D. A. Cremers, R. C. Chinni, *Appl. Spectrosc. Rev.*, 2009, **44**, 457-506.

10 N. E. Widjonarko, J. D. Perkins, J. E. Leisch, P. A. Parilla, C. J. Curtis, D. S. Ginley, J. J. Berry, *Rev. Sci. Instrum.*, 2010, **81**, 073103.

11 B. Le Drogoff, M. Chaker, M. Sabsabi, O. Barthélemy, T. W. Johnston, S. Laville, and F. Vidal, *Appl. Spectrosc.*, 2004, **58**(1), 122-129.

12 Dong-Hyoung Lee, Sol-Chan Han, Tae-Hyeong Kim, and Jong-il Yun, *Anal. Chem.*, 2011, **93**, 9456-9461.

13 M. Mueller, I. B. Bornushkin, S. Florek, D. Mory, U. Panne, *Anal. Chem.*, 2007, **79**, 4419-4426.

14 Vasily Lednev, Sergey M. Pershin, Alexey F. Bunkin, *J. Anal. At. Spectrom.*, 2010, **25**, 1745-1757.

15 Jie Li, Jidong Lu, Zhaoxiang Lin, Shunsheng Gong, Chengli Xie, Liang Chang, Lifei Yang, Pengyan Li, *Opt. Laser Technol.*, 2009, **41**, 907-913.

16 B. C. Castle, K. Talabardon, B. W. Smith, J. D. Winefordner, *Appl. Spectrosc.*, 1998, **52**(5), 649-657.

17 S. Darwiche, M. Benmansour, N. Eliezer, D. Morvan, *Spectrochim. Acta Part B*, 2010, **65**, 738-743.

18 L. M. Cabalín, D. Romero, C. C. García, J. M. Baena, J. J. Laserna, *Anal. Bioanal. Chem.*, 2002, **372**, 352-359.

19 L. A. Alvarez-Trujillo, A. Ferreo, J. J. Laserna, *J. Anal. At. Sepctrom.*, 2008, **23**, 885-888.

20 L. A. Alvarez-Trujillo, A. Ferreo, J. J. Laserna, D. W. Hahn, *Appl. Spectrosc.*, 2008, **62**(10), 1144-1152.

21 David Dussault, Paul Hoess, *Proc. SPIE*, 2004, **5563**, 195-204.

22 J. M. Mermet, P. Mauchien, J. L. Lacour, *Spectrochim. Acta Part B*, 2008, **63**, 999-1005.

23 A. Frenkel, M. A. Sartor, M. S. Wlodawski, *Appl. Opt.*, 1997, **36**, 5288-5297.

24 M. C. Teich, B. E. A. Saleh, *Opt. Lett.*, 1982, **7**, 365-367.

25 *RCA Photomultiplier Manual*, RCA Electronic Components, Harrison, N.J., 1970.

26 J. R. Prescott, *Nucl. Instrum. Methods*, 1966, **39**, 173-179.

27 Eloísa Díaz-Francés, Francisco J. Rubio, *Stat. Papers*, 2013, **54**, 309-323.

28 K. Krishnamoorthy, *Hanbook of Statistical Distributions with Applications*, Chapman & Hall/CRC, Tayor & Francis Group: Boca Raton, 2006.

29 Chan-Kyu Kim, Jung-Hwan In, Seok-Hee Lee, Sungho Jeong, *Opt. Lett.*, 2013, **38**, 3032-3035.

30 Chan-Kyu Kim, Seok-Hee Lee, Jung-Hwan In, Hak-Jae Lee, Sungho Jeong, *Opt. Express*, 2013, **21**, A1018-A1027.

31 V. K. Unnikrishnan, Kamlesh Alti, V. B. Kartha, C. Santhosh, G. P. Gupta, B. M. Suri, *Pramana-J. Phys.*, 2010, **74**, 983-993.
32 Yong-Ill Lee, Kyuseok Song, Hyong-Ki Cha, Jong-Min Lee, Min-Chun Park, Gae-Ho Lee, Joseph Sneddon, *Appl. Spectrosc.*, 1997, **51**, 959-964.
33 Yu Li, Changhong Hu, Hanzhuang Zhang, Zhankui Jiang, Zhongshan Li, *Appl. Opt.*, 2009, **48**, B105-B110.
34 National Institute of Standards and Technology (NIST), http://physics.nist.gov/PhysRefData/ASD/lines_form.html, (accessed March 2014).
35 National Institute of Standards and Technology (NIST), http://physics.nist.gov/PhysRefData/ASD/levels_form.html, (accessed March 2014).
36 Timothy C. Williams, Christopher R. Shaddix, *Rev. Sci. Instrum.*, 2007, **78**, 123702.
37 Andrzej W. Miziolek, Vincenzo Palleschi, Israel Schechter, *Laser-Induced Breakdown Spectroscopy (LIBS): Fundamentals and Applications*, Cambridge University Press, New York, 2006, ch. 3, pp. 122-170.
38 F. Bredice, F. O. Borges, H. Sobral, M. Villagran-Muniz, H.O. Di Rocco, G. Cristoforetti, S. Legnaioli, V. Palleschi, L. Pardini, A. Salvetti and E. Tognoni, *Spectrochim. Acta Part B*, 2006, **61**, 1294-1303.
39 A. M. El Sherbini, Th. M. El Sherbini, H. Hegazy, G. Cristoforetti, S. Legnaioli, V. Palleschi, L. Pardini, A. Salvetti and E. Tognoni, *Spectrochim. Acta Part B*, 2005, **60**, 1573-1579.